Possibility of QCD critical point sweep during black hole formation [☆]

A. Ohnishi[a], H. Ueda[b], T. Z. Nakano[a,b], M. Ruggieri[a], K. Sumiyoshi[c]

[a]*Yukawa Institute for Theoretical Physics, Kyoto University, Kyoto 606-8502, Japan*
[b]*Department of Physics, Faculty of Science, Kyoto University, Kyoto 606-8502, Japan*
[c]*Numazu College of Technology, Ooka 3600, Numazu, Shizuoka 410-8501, Japan*

Abstract

We discuss the possibility to probe the QCD critical point during the dynamical black hole formation from a gravitational collapse of a massive star, where the temperature and the baryon chemical potential become as high as $T \sim 90$ MeV and $\mu_B \sim 1300$ MeV. Comparison with the phase boundary in chiral effective models suggests that quark matter is likely to be formed before the horizon is formed. Furthermore, the QCD critical point may be probed during the black hole formation. The critical point is found to move in the lower temperature direction in asymmetric nuclear matter, and in some of the chiral models it is found to be in the reachable region during the black hole formation processes.

Keywords: critical point, QCD phase diagram, black hole formation, chiral effective model, neutrino-radiation hydrodynamics

1. Introduction

The critical point (CP) of the Quantum Chromodynamics (QCD) [1] may be regarded as a corner stone of the QCD phase diagram; the cross over [2] and the first order phase boundaries between the hadron and quark-gluon phases are connected by CP, then it determines the global structure of the phase diagram. Against its importance, the existence, number and location of CP are not yet established in theoretical calculations. The sign problem makes the lattice Monte Carlo simulation difficult in the large baryon-chemical potential (μ_B) region [3], the strong coupling expansion of lattice QCD [4] is not yet reliable to describe the real world, and the predictions in effective models are spread in the $T - \mu_B$ plane [5]. Thus further experimental and theoretical developments are necessary to reveal the properties of CP. The search for CP in heavy ion collisions is ongoing in the beam energy scan programs at RHIC [6], and CP is one of the most important targets in the forthcoming FAIR facility. The most characteristic feature of CP is the divergence of the coherence length ξ. The phase transition becomes the second order, and large fluctuations of the order parameters are expected in a volume of the size ξ^3. On the basis of this idea, various signatures of CP have been suggested theoretically [7]. However, since the system size and the evolution time are limited, it is not an easy task to observe the divergence signature of ξ in heavy-ion collisions [8]. In addition, if the baryon chemical potential of CP (μ_{CP}) is above 500 MeV, CP may not be reachable in heavy-ion collisions. Therefore, it is important to examine other candidate sites where hot and dense matter is formed and CP is reachable.

A gravitational collapse of a massive star may be one of the promising candidates for the CP hunting. It has been argued that the transition to quark matter might trigger the second collapse and bang in supernova explosions [9, 10]. Recent calculation suggests that the QCD phase transition may take place during the core-collapse of a star with $M = (10 - 15)M_\odot$ when one uses the relativistic equation of state (Shen EOS) [11] combined with the bag model EOS at high T or ρ_B for a small bag constant, $B^{1/4} \simeq 162$ MeV [10]. The QCD phase transition leads to the second shock, and is suggested to give successful supernova explosion even in a simulation with spherical symmetry. Non-rotating massive stars with mass $M \gtrsim 20M_\odot$ are expected to collapse without supernova explosions and to form a black hole (BH) [12]. In Refs. [13, 14, 15], the BH formation processes are calculated by using the neutrino-radiation hydrodynamical simulations in general relativity. In the collapse and bounce stage of a $40M_\odot$ star, the core bounce launches the shock wave, but the shock wave stalls due to the collisions with falling matter (accretion) and goes down to the surface of the compact object. The proto-neutron star is born at center and gradually contracts. Because of the accretion, the proto-neutron star mass increases rapidly and reaches the critical mass. The dynamical collapse occurs again at this point and the BH is formed at 1.3 s after the bounce in the case of the Shen EOS [11]. If we adopt a relativistic EOS with hyperons (Ishizuka EOS) [16] or the Lattimer-Swesty EOS [17], the second collapse becomes more rapid (~ 0.7 s after the bounce), while the average neutrino energies are lower with Ishizuka EOS [15]. The combination of the neutrino duration time and the neutrino energy may be used as a signal of the hyperon emergence or other new degrees of freedom during the BH formation [18].

During the BH formation, hot ($T \sim 90$ MeV) and dense ($\rho_B \sim 4\rho_0$) matter is created. The temperature and density in

BH formation are significantly higher than those in the model explosion calculation of supernova, where the highest temperature and density are $(T, \rho_B) \sim (21.5 \text{ MeV}, 0.24 \text{ fm}^{-3})$ [16]. In hotter and denser environment during BH formation compared with the supernova explosions, we have a larger possibility of creating a new form of matter, such as the dense quark matter. Thermodynamical variables at a given time vary as a function of radius in a proto-neutron star and form a line in the $T - \mu_B$ plane. This thermodynamical line, referred to as the BH formation profile in the later discussions, evolves with time and may pass through CP and the vicinity. We call here this situation as the *CP sweep*.

In this Letter, we examine the location of the QCD phase boundary and CP in two-flavor chiral effective models at finite isospin chemical potential $\delta\mu \equiv (\mu_d - \mu_u)/2$, and discuss the possibility of the CP sweep during the BH formation from a gravitational collapse of a massive star. First, we compute the CP location in the $T - \mu_B$ plane in chiral effective models such as the Nambu-Jona Lasinio (NJL) model [19], the Polyakov loop extended Nambu-Jona-Lasino (P-NJL) model [20, 21, 22], P-NJL model with eight-quark interaction [23], and the Polyakov loop extended quark-meson (PQM) model [24, 25]. The bag model EOS adopted in Ref. [10] is not suited to the present purpose, since it does not have CP. In the dynamical BH formation, we have abundant neutrinos, and approximate β equilibrium including neutrinos are realized inside the neutrino sphere, $\mu_n - \mu_p = \mu_e - \mu_\nu$, while neutrinos are out of equilibrium outside. In both cases, it is necessary to take account of finite isospin chemical potential $\delta\mu$ as another independent thermodynamical variable [26], rather than imposing the neutrino-less β equilibrium condition ($\delta\mu = \mu_e/2$) in order to examine the CP property during the BH formation. Recently, P-NJL model with isospin chemical potential has been investigated with [27] and without [28] neutrino-less β equilibrium conditions. At finite $\delta\mu$, we naively expect that CP moves in the lower T direction because of the larger d-quark chemical potential $\mu_d = \mu_B/3 + \delta\mu$. Since the matter passes through the high μ_B and low T region, the reduction of the CP temperature T_{CP} is essential for the CP sweep during the BH formation. Next, we compare the results of the CP location in the chiral effective models with the evolution of thermodynamical variables $(T, \mu_B, \delta\mu)$ during the BH formation obtained in Ref. [13]. It should be noted that we compare the results of the CP location in chiral effective models and the thermodynamical condition (T, μ_B) calculated with the hadronic EOS. This comparison is relevant, since the thermal trajectory should be the same even if we use the combined EOS of quark and hadronic matter, as long as the hadronic EOS is reproduced at low T and μ_B in the combined EOS. Finally, we discuss the possibility of the CP sweep during the BH formation from the above comparison.

2. Polyakov loop extended chiral effective models

In this section, we summarize the chiral effective models, the NJL, P-NJL, and PQM models, which we use in computing the CP location in the $T - \mu_B$ plane.

2.1. NJL model

The Lagrangian density of the two flavor NJL model is given by

$$\mathcal{L}_{\text{NJL}} = \bar{q}\left(i\gamma^\mu\partial_\mu - m_0\right)q + G_\sigma\left[(\bar{q}q)^2 + (\bar{q}i\gamma_5\boldsymbol{\tau}q)^2\right]$$
$$- G_\rho\left[(\bar{q}\gamma^\mu\boldsymbol{\tau}q)^2 + (\bar{q}i\gamma_5\gamma^\mu\boldsymbol{\tau}q)^2\right] - G_\omega\left[(\bar{q}\gamma^\mu q)^2 + (\bar{q}i\gamma_5\gamma^\mu q)^2\right], \quad (1)$$

where q denotes a quark field with Dirac, color and flavor indices; $\boldsymbol{\tau}$ is the Pauli matrices in the flavor space. In what follows, we take $G_\rho = G_\omega \equiv G_V$, which amounts to take ω and $\boldsymbol{\rho}$ mesons degenerate in the vacuum. We can fix the value of G_S by fitting the well known properties of the QCD vacuum. We will take the ratio G_V/G_S as a free parameter.

We are interested in unbalanced populations of u and d quarks, not in the neutrino-less β-equilibrium. For this reason, we introduce two independent chemical potentials for u and d quarks. At the mean field level, the effect of the vector interaction is to shift the quark chemical potentials: the flavor singlet interaction gives a contribution proportional to $\rho_u + \rho_d$; on the other hand, the flavor triplet interaction gives a contribution proportional to the isospin density, $\rho_u - \rho_d$. Keeping this into account, and for later convenience, we define

$$\tilde{\mu}_u = \mu - \delta\mu - 4G_V\rho_u, \quad \tilde{\mu}_d = \mu + \delta\mu - 4G_V\rho_d, \quad (2)$$

where μ and $\delta\mu$ represent chemical potentials conjugated to the total quark number density and to isospin density, respectively.

The one-loop thermodynamic potential can be represented as the sum of the the vacuum Ω_0 and the thermal (finite temperature and finite chemical) Ω_T contributions,

$$\Omega_{\text{NJL}} = \Omega_0 + \Omega_T, \quad (3)$$

$$\Omega_0 = \frac{\Sigma^2}{4G_\sigma} - 2N_c\sum_f\int\frac{d^3\boldsymbol{p}}{(2\pi)^3}F(\boldsymbol{p}^2, \Lambda)E_p, \quad (4)$$

$$\Omega_T = -2TN_c\sum_f\int\frac{d^3\boldsymbol{p}}{(2\pi)^3}\log\left(1 + e^{-\beta\mathcal{E}_+^f}\right)\left(1 + e^{-\beta\mathcal{E}_-^f}\right)$$
$$- 2G_V\left(\rho_u^2 + \rho_d^2\right), \quad (5)$$

$$\mathcal{E}_\pm^f = E_p \pm \tilde{\mu}_f, \quad (6)$$

where $E_p = \sqrt{\boldsymbol{p}^2 + M^2}$ with $M = m_0 + \Sigma$, and $\Sigma \equiv -2G_\sigma\langle\bar{q}q\rangle$ corresponds to the mean field quark self-energy. In Eq. (4), we have treated the ultraviolet divergence of the vacuum energy by the use of a smooth regulating function, $F(\boldsymbol{p}^2, \Lambda) = [1 + (\boldsymbol{p}^2)^5/\Lambda^{10}]^{-1}$. This is done just for numerical convenience; quantitatively, we have checked that the results are consistent with the more common hard cutoff regularization scheme, within a few percent. The thermal part Ω_T is a finite contribution which does not need any regularization.

2.2. The P-NJL model

The P-NJL model Lagrangian density is still specified by Eq. (1), with the derivative replaced by a covariant one: $\partial_\mu \to D_\mu = \partial_\mu - iA_\mu$. Here, A_μ is a temporal, static and homogeneous

background gluon field related to the Polyakov loop P, whose expectation value is computed self-consistently. The one-loop thermodynamic potential in Eq. (3) is replaced with [21]

$$\Omega_{\text{P-NJL}} = \Omega_0 + \Omega_T + \mathcal{U}(P, \bar{P}, T) , \tag{7}$$

$$\mathcal{U}[P, \bar{P}, T] = T^4 \left\{ -\frac{a(T)}{2} \bar{P}P + b(T) \ln H(P, \bar{P}) \right\} , \tag{8}$$

$$P = \frac{1}{N_c} \text{Tr} \left[\mathcal{P} \exp\left(i \int_0^\beta d\tau A_4 \right) \right] \equiv \frac{1}{3} \text{Tr} e^{i\phi/T} , \tag{9}$$

where $\mathcal{U}(P, \bar{P}, T)$ is the Polyakov loop effective potential [22] with $H(P, \bar{P}) = 1 - 6\bar{P}P + 4(\bar{P}^3 + P^3) - 3(\bar{P}P)^2$, $a(T) = a_0 + a_1(T_0/T) + a_2(T_0/T)^2$, and $b(T) = b_3(T_0/T)^3$. We adopt the Polyakov gauge, where ϕ is specified by $\phi = \phi_3\lambda_3 + \phi_8\lambda_8$. The standard choice of the parameters reads [22] $a_0 = 3.51$, $a_1 = -2.47$, $a_2 = 15.2$, $b_3 = -1.75$. The parameter T_0 in Eq. (8) sets the deconfinement scale in the pure gauge theory, i.e. $T_c = 270$ MeV.

The thermal part of the thermodynamic potential is now given by [21]

$$\Omega_T = -2G_V\left(\rho_u^2 + \rho_d^2\right) - 2T \sum_f \int \frac{d^3p}{(2\pi)^3} \log\left(F_+^f F_-^f\right) , \tag{10}$$

$$F_+^f = 1 + 3\bar{P}e^{-\beta\mathcal{E}_+^f} + 3Pe^{-2\beta\mathcal{E}_+^f} + e^{-3\beta\mathcal{E}_+^f} , \tag{11}$$

$$F_-^f = 1 + 3Pe^{-\beta\mathcal{E}_-^f} + 3\bar{P}e^{-2\beta\mathcal{E}_-^f} + e^{-3\beta\mathcal{E}_-^f} . \tag{12}$$

In Eq. (11), the addenda on the r.h.s. correspond to the thermal contribution of zero, one, two and three quark states, respectively. Analogously, Eq. (12) is the thermal contribution of antiquarks.

2.3. P-NJL model with eight-quark interaction (P-NJL$_8$)

With eight-quark interaction, the quark Lagrangian is [23]

$$\mathcal{L} = \mathcal{L}_{\text{NJL}} + G_{\sigma 8}\left[(\bar{q}q)^2 + (\bar{q}i\gamma_5\tau q)^2\right]^2 . \tag{13}$$

We do not include here the eight-quark interaction in the vector channel. The one loop thermodynamic potential is still given by Eq. (7), with

$$\Omega_0 = \frac{3G_{\sigma 8}}{16G_\sigma^4}\Sigma^4 + \frac{\Sigma^2}{4G_\sigma} - 2N_c \sum_f \int \frac{d^3p}{(2\pi)^3} F(p^2, \Lambda)E_p , \tag{14}$$

and $E_p = \sqrt{p^2 + M^2}$, with $M = m_0 + \Sigma + \Sigma^3(G_{\sigma 8}/2G_\sigma^3)$. For simplicity, we call this model P-NJL$_8$.

P-NJL$_8$ parameters $(\Lambda, G_\sigma, G_{\sigma 8}, m_0)$ are determined to fix f_π, m_π, m_σ, and $\langle \bar{u}u \rangle$, and as a result, the chiral and deconfinement transition temperatures are found to roughly agree [23]. The eight-quark interaction is found to make chiral cross over sharper at $\mu = 0$; μ makes this cross over stronger, and eventually leads to the first order transition. Hence eight-quark interaction causes chemical potential of CP to be smaller.

2.4. PQM model

The Lagrangian density of the PQM model is given by

$$\mathcal{L} = \bar{q}\left[i\gamma^\mu D_\mu - g(\sigma + i\gamma_5\tau \cdot \pi) - g_v\gamma^\mu(\omega_\mu + \tau \cdot R_\mu)\right]q$$
$$+ \frac{1}{2}(\partial_\mu\sigma)^2 + \frac{1}{2}(\partial_\mu\pi)^2 - U(\sigma, \pi) - \mathcal{U}(P, \bar{P}, T)$$
$$- \frac{1}{4}\omega_{\mu\nu}\omega^{\mu\nu} - \frac{1}{4}R_{\mu\nu} \cdot R^{\mu\nu} + \frac{1}{2}m_v^2(\omega_\mu\omega^\mu + R_\mu \cdot R^\mu) . \tag{15}$$

The mesonic potential is $U(\sigma, \pi) = \lambda\left(\sigma^2 + \pi^2 - v^2\right)^2/4 - h\sigma$, and $\omega_{\mu\nu}$ and $R_{\mu\nu}$ are the field tensors of the ω and ρ mesons. We use the same Polyakov loop effective potential as that in the P-NJL model, Eq. (8). In the mean field approximation, the thermodynamic potential is given by

$$\Omega_{\text{PQM}} = \mathcal{U}(P, \bar{P}, T) + U(\sigma, \pi = 0) + \Omega_0 + \Omega_T , \tag{16}$$

$$\Omega_0 = -2N_fN_c \int \frac{d^3p}{(2\pi)^3} E_p\theta(\Lambda^2 - p^2) , \tag{17}$$

where Ω_0 corresponds to the regularized fermion vacuum energy with $M = g\sigma$, and Ω_T is still given by Eq. (10) with $G_V = g_v^2/2m_v^2$. While the PQM model is renormalizable and an elegant procedure of dimensional renormalization is feasible [25], it is enough to cut large momenta by a hard cutoff for our purposes.

2.5. Model parameterization

In this study, we fix μ and $\delta\mu$, and compute ρ_u, ρ_d, the chiral condensate and the Polyakov loop expectation values self-consistently, requiring the stationary condition of the thermodynamic potential. In the case of the NJL model and the P-NJL model without eight-quark interaction, the parameters G_σ, Λ and m_0 are chosen in order to reproduce the QCD vacuum properties $\langle \bar{u}u \rangle = (-250 \text{ MeV})^3$, $f_\pi = 92.4$ MeV and $m_\pi = 139$ MeV. They are given as $\Lambda = 618.98$ MeV, $G_\sigma = 2.05/\Lambda^2$, and $m_0 = 5.28$ MeV. The parameter T_0 in the Polyakov loop effective potential is taken to be $T_0 = 210$ MeV. With this parameter choice, the constituent quark mass in the vacuum is $M \approx 340$ MeV. In P-NJL$_8$, we use the parameterization in [23], $\Lambda = 631.5$ MeV, $G_\sigma = 1.864/\Lambda^2$, $G_{\sigma 8} = 11.435/\Lambda^8$, and $m_0 = 5.5$ MeV, which give the vacuum constituent quark mass $M \approx 353$ MeV. For G_V, estimates exist based on perturbative one gluon exchange [29], $r \equiv G_V/G_\sigma = 0.5$; on instanton-anti-instanton molecule model [30], $r = 0.25$; and an interpolation is obtained by a fit of the Lattice data with the P-NJL$_8$ model in [31], $r = 1$. We here treat r as a free parameter, and compare the results with $r = 0$ and $r = 0.2$.

The parameters of the PQM model, v, λ, g and h, are fixed to reproduce some vacuum properties: the chiral condensate in the vacuum, $\sigma = f_\pi = 92.4$ MeV; the vacuum pion mass, $m_\pi^2 = h/f_\pi = (139\text{MeV})^2$; the constituent vacuum quark mass, $M = gf_\pi = 335$MeV; the sigma mass, given by $m_\sigma^2 = \partial^2\Omega/\partial\sigma^2 = (700 \text{ MeV})^2$. In this article, we use the following parameter set: $\Lambda = 600$MeV, $v^2 = -(617.68\text{MeV})^2$, and $\lambda = 2.7255$. We use the same Polyakov loop effective potential as that in the P-NJL model. The vector meson mass is chosen to be $m_v =$

770 MeV. The vector coupling is treated as a free parameter, and we compare the results with $r = g_v/g = 0$ and 0.2 in the later discussions.

P-NJL models with $SU(3)_f$ are known to support hybrid neutron star mass of 1.74-2.12 $M_\odot$ when combined with a hadronic EOS at low densities [32]. By comparison, an $SU(3)_f$ version of PQM model connected with a hadronic EOS can support the hybrid neutron star mass of $2.0M_\odot$ [33]. Generally speaking, the EOS becomes softer with larger degrees of freedom, then $SU(2)_f$ versions of these models are expected to give stiffer EOS than in $SU(3)_f$. Therefore $SU(2)_f$ chiral effective models adopted in this work would result in larger maximum masses of neutron stars, which are consistent with the recently observed $1.97 \pm 0.04M_\odot$ neutron star [34].

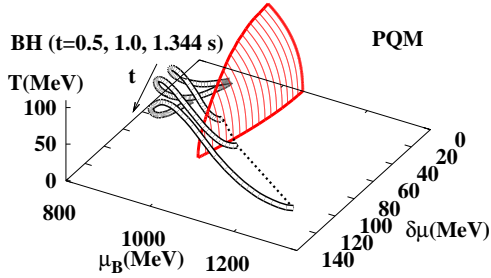## 3. Critical point location and its sweeping

Figure 1: Phase diagram in $(T, \mu_B, \delta\mu)$ space. First order phase boundaries (T, μ_B) calculated with PQM are shown for several values of the isospin chemical potential, $\delta\mu$. We also show the BH formation profile, (thermodynamical profile $(T, \mu_B, \delta\mu)$ during the BH formation) at $t = 0.5, 1.0, 1.344$ sec after the bounce (double lines).

3.1. Critical point and phase boundary in asymmetric matter

In Fig. 1, we show the isospin chemical potential dependence of the first order phase boundary and the critical point in the PQM model. We find a trend that the first order phase boundary shrinks at finite isospin chemical potential. Transition temperature at a given baryon chemical potential $\mu_B = 3\mu$ decreases, and the transition chemical potential μ_c at $T = 0$ also decreases. We do not consider here the pion condensed phase, because the s-wave pion condensation will not be realized when we include the s-wave πN repulsion [35]. The CP location is sensitive to $\delta\mu$. Compared with the results in symmetric matter, T_{CP} becomes smaller at finite $\delta\mu$ and reaches zero at $\delta\mu = \delta\mu_c \simeq (50 - 80)$ MeV. The downward shift of T_{CP} may be understood from the density shift. At low T and without the vector interaction, the quark density is proportional to μ^3, $\rho_{u,d} \propto (\mu \mp \delta\mu)^3$. Then the sum of u and d quark density increases when $\delta\mu$ is finite, and it simulates higher μ, where the transition temperature is lower.

Table 1: Location of CP, the transition chemical potential at $T = 0$ (μ_c), and the type of the transition to quark matter during the BH formation. All T and μ values are given in the unit of MeV.

Model	r	$\delta\mu$	T_{CP}	μ_{CP}	μ_c	BH
NJL	0	0	50	993	1095	
		50	45	999	1065	CP sweep
		65	37	1005	1035	
	0.2	0	22	1095	1110	
		50	10	1073	1074	Cross over
P-NJL	0	0	106	975	1095	
		50	92	990	1065	CP sweep
		65	86	996	1035	
	0.2	0	74	1062	1110	
		50	39	1068	1086	Cross over
P-NJL$_8$	0	0	145	600	1005	
		50	125	678	900	First order
		65	118	690	870	
	0.2	0	129	708	1020	
		50	119	720	930	First order
PQM	0	0	105	964	1046	
		50	87	979	1025	CP sweep
		70	62	989	1007	
	0.2	0	91	1006	1057	
		50	69	1016	1040	CP sweep
		70	35	1020	1024	

In Table 1, we summarize the CP location (T, μ_B) for several values of $\delta\mu$ and $r = G_V/G_\sigma$ in NJL, P-NJL, P-NJL$_8$, and PQM models. In P-NJL$_8$, our results at $r = 0$ are in agreement with those in Ref. [28]. The transition chemical potential at $T = 0$ is in the range of 1000 MeV $< \mu_c <$ 1110 MeV. μ_c is sensitive to the details of the interaction, especially to the strength of the vector interaction. The temporal component of the vector potential shifts the chemical potential effectively as already introduced in Eq. (2). In the momentum integral, we find the effective chemical potential $\tilde{\mu}_f = \mu \mp \delta\mu - V_f$ appears, where $V_f = 4G_V\rho_f$ represents the vector potential for quarks. The repulsive vector potential reduces the effects of the chemical potential and consequently leads to an upward shift of μ_c by about 10-15 MeV at $r = 0.2$. When we increase the vector coupling from $r = 0$ to $r = 0.2$ in NJL, the first order transition boundary is shifted upward in μ and T_{CP} is reduced from 50 MeV to 22 MeV. At larger vector coupling, the first order phase boundary disappears, and the QCD phase transition becomes the cross over at any μ. This trend also applies to the P-NJL and PQM models; the phase boundary is shifted in the larger μ direction and shrinks in the T direction with finite vector interaction. In P-NJL$_8$, the first order phase transition is robust and survives with larger vector interaction such as $r = 0.8$, while the effects of the vector interaction is qualitatively the same.

3.2. BH formation profile

In Fig. 2, we show the BH formation profile $(T, \mu_B, \delta\mu)$ [13] calculated by using the Shen EOS at $t = 0.5, 1.0$ and 1.344 sec
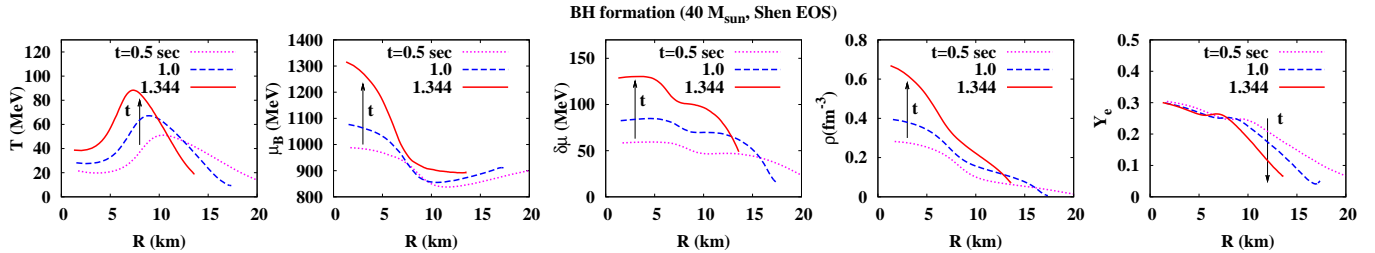
4

Figure 2: The BH formation profile, $(T, \mu_B, \delta\mu)$, as a function of the radius. We also show the baryon density (ρ_B) and the electron fraction ($Y_e \equiv \rho_e/\rho_B$). Results are shown for the gravitational collapse of a 40 $M_\odot$ star at $t = 0.5$ sec (dotted lines), 1.0 sec (dashed lines), and 1.344 sec (solid lines, just before the horizon formation).

after the bounce during the BH formation from a 40 $M_\odot$ star in the proto-neutron star core, where the mass coordinate from the center is $M < 1.6M_\odot$. The time $t = 1.344$ sec is just before the horizon formation. From the outer to the inner region of the proto-neutron star, T first increases from $T \sim 10$ MeV to $T \sim (50 - 90)$ MeV in the middle heated region, and decreases again inside. The central density grows from $\rho_B \sim \rho_0$ at bounce to $2\rho_0$, $2.5\rho_0$ and $4\rho_0$ at 0.5, 1.0 and 1.344 sec, respectively. The charge to baryon ratio (Y_e) is less than 0.3 inside the proto-neutron star [14]. The isospin chemical potential is found to be $50 - 130$ MeV in the inner region. The baryon chemical potential μ_B is found to go over 1300 MeV in the central region just before the horizon formation at $t = 1.344$ sec.

The maximum chemical potential is much larger than the $\Lambda(1115)$ mass, and hyperons are expected to emerge. Actually, hyperons are formed abundantly when we use Ishizuka EOS including hyperons [15], while the proto-neutron star collapses earlier and the maximum μ_B (~ 1100 MeV) is lower.

It should be noted that the maximum mass of neutron stars is 2.17 $M_\odot$ in Shen EOS, which does not contradict to the observation of $1.97M_\odot$ neutron star [34]. We need care in discussing the results of Ishizuka EOS, since the maximum mass is $1.63M_\odot$ and it cannot support the $1.97M_\odot$ mass neutron star. It would be important to discuss the hyperon admixture with more repulsive hyperon potentials at high densities, which support heavier neutron stars.

3.3. Possibility of critical point sweep

We shall now compare the CP location and the phase boundary with the BH formation profile. In Fig. 3, we compare the phase boundaries and the CP location in NJL (left-top), P-NJL (right-top), P-NJL$_8$ (left-bottom) and PQM (right-bottom) models with the BH formation profile, (T, μ_B). As already mentioned, the transition chemical potential is in the range of 1000 MeV $< \mu_c <$ 1110 MeV in symmetric nuclear matter, and it decreases at finite $\delta\mu$. During the BH formation, the baryon chemical potential reaches around 1000, 1100 and 1300 MeV in the central region of the proto-neutron star at $t = 0.5, 1.0$ and 1.344 sec, respectively. This comparison suggests that quark matter would be formed between $t = 0.5$ and 1.0 sec in the central region of the proto-neutron star in most of the models considered here.

Since the CP location has strong dependence on model and parameter, there are three possible types in the transition to the

quark matter during the evolution of matter toward the BH formation; the first order transition, the cross over transition, and the CP sweep. In P-NJL$_8$ (with and without vector interaction), T_{CP} is relatively high even in asymmetric matter, then the matter experiences the first order phase transition, and CP is not reached. In NJL and P-NJL with vector interaction, T_{CP} decreases in asymmetric matter, and CP already disappears in the central region at $t = 1.0$ sec, where the isospin chemical potential is large, $\delta\mu \sim 70$ MeV. In this case, the BH formation profiile evolves above CP, and the cross over transition to quark matter will proceed without going through the first order boundary. In NJL and P-NJL models without vector interaction and PQM with and without vector interaction, the BH formation profile goes through CP from below, as shown in the double line in Fig. 1. CP in symmetric matter is above the BH formation profile at $t = 1.0$ sec, while CP in asymmetric matter is below the line at $t = 1.344$ sec. Since the matter in the central region is highly asymmetric ($\delta\mu = (50 - 130)$ MeV) at $t = 1.344$ sec, some part of the off-center BH forming matter would go through CP between $t = 1$ and 1.344 sec, *i.e.* CP is swept.

CP sweep will take place in the off-center inner core. As can be seen in Fig. 2, the highest density and baryon chemical potential is realized at center, while temperature becomes highest off-center due to the shock wave. In the PQM ($r = 0$) case, as a typical example of CP sweep, the quark matter formation takes place first at center with $T < T_{CP}$, the quark matter region grows, and the CP sweep takes place when the boundary temperature reaches T_{CP}. We find from Fig. 3 that CP will be swept at a little inner region than the highest T radius, and this corresponds to $R = 6 - 8$ km as seen in Fig. 2.

It is also interesting to discuss whether the condition in core-collapse supernovae may cross the phase boundaries to the quark matter phase. We examined the numerical result of the gravitational collapse and bounce from the massive star of $15M_\odot$ with Shen-EOS [36]. The density and temperature at the core bounce are $(\rho_B, T) = (0.2\text{fm}^{-3}, 15$ MeV) at center. The baryon chemical potential and temperature do not reach the phase transition region in this case. They do not rise enough during the stage of the stalled shock wave for 200 ms after the core bounce. Therefore, it is not likely to have the CP sweep in dense matter around the core bounce for successful explosions. The situation is similar in the numerical result of adiabatic col-
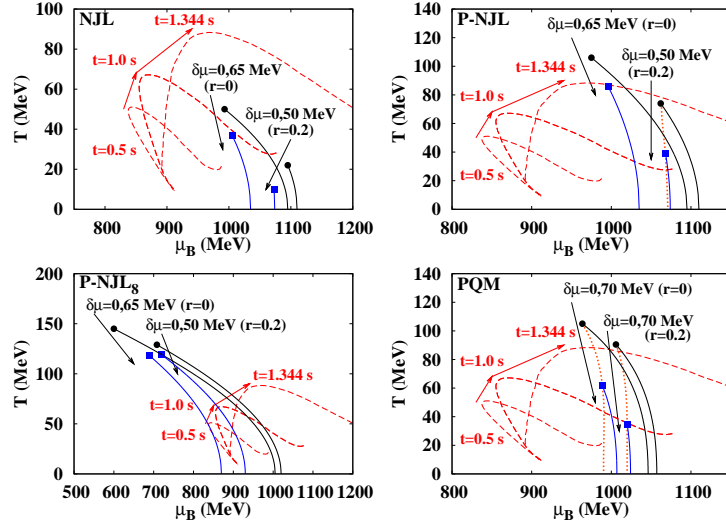
5

Figure 3: Critical point, phase boundary and the BH formation profile. Critical point in symmetric (circles) and asymmetric (squares) matter and the first order phase transition boundaries (solid lines) in chiral effective models are compared with the BH formation profile (T, μ_B) at $t = 0.5$, 1.0 and 1.344 sec (dashed lines). Top-left, top-right, bottom-left and bottom-right panels show the results in the NJL, P-NJL, P-NJL$_8$, and PQM models, respectively. We show the results without $(r = 0)$ and with $(r > 0)$ vector interaction. In P-NJL with vector interaction and PQM, we also show the CP trajectory (dotted lines). Arrows around the BH formation profile show time evolution, and arrows around the critical points show the isospin chemical potential dependence.

lapse and bounce of the 15M$_\odot$ star using Ishizuka' hyperonic EOS as discussed in [16]. However, there are still possibilities to have the quark matter and the CP sweep in the late stage of core-collapse supernovae. In the thermal evolution of the proto-neutron star for ~ 20 sec after the birth in supernovae, the density and temperature increase further due to the contraction during the thermal evolution. In fact, the condition may become closer to that of CP in the long term evolution after the bounce [36]. In the massive proto-neutron star cases [37], hyperons and quarks appear in the late stage due to the extreme conditions, where they reach the phase boundaries. Hence, the CP sweep may be realized in the evolution toward the black hole formation in the very massive proto-neutron stars, while the explosion goes on. It is also possible to have high density and temperature in the transition region to quark matter at the second bounce of the core collapse supernova when one adopts an EOS having a low transition baryon chemical potential [10].

There are two comments in order. (a) While we have compared the CP location and the BH formation profile in $(T, \mu_B, \delta\mu)$, the relation between the densities and chemical potentials is highly model dependent and the baryon densities in the quark and hadronic models considered here do not generally coincide; For example, in NJL and P-NJL, the baryon densities on CP are found to be $\rho_B = 0.30$ and 0.29 fm^{-3} at $\delta\mu = 65$ MeV, respectively, while $\rho_B = 0.36$ and 0.31 fm^{-3} in Shen EOS at the corresponding $(T, \rho_B, \delta\mu)$. In PQM with $r = 0$ and 0.2, $\rho_B = 0.25$ and 0.23 fm^{-3} at $\delta\mu = 60$ MeV, respectively, while $\rho_B = 0.33$ and 0.34 fm^{-3} in Shen EOS on these points. Thus the baryon densities in chiral effective and hadronic models have $10-50\%$ differences in density at CP, and the results shown in this article would be modified when we perform a consistent calculation using a hybrid supernova matter

EOS which smoothly connect quark and hadronic matter EOSs. However, the trajectories span a wide region in (T, ρ_B) which are in a range expected for the phase transition lines and CP, then we expect the CP sweep or at least the transition to quark matter even in a consistent calculation of the black hole formation. (b) The symmetry energy in RMF models has a strong dependence in ρ_B and may overestimate the effects at high densities. When one adopts a weak ρ_B dependence of the symmetry energy at high densities, smaller isospin chemical potential results. In this case, the cross over transition during BH formation becomes less probable, since T_{CP} is kept to be high at small $\delta\mu$.

4. Summary

In this Letter, we have discussed the possibility of the QCD phase transition to quark matter and the critical point (CP) sweep during the dynamical black hole (BH) formation. We have compared the phase boundary and CP in chiral effective models with the BH formation profile, thermodynamical variables (T, μ_B) calculated in the neutrino-radiation hydrodynamics. For this comparison, it is necessary to consider asymmetric matter at finite isospin chemical potential, $\delta\mu = (\mu_n - \mu_p)/2 \neq 0$. The isospin chemical potential is found to reduce the temperature of the critical point T_{CP}, then we have a larger possibility of the CP sweep or the cross over transition to quark matter.

In the chiral effective models considered here, with and without the vector interaction, the transition chemical potential at $T = 0$ is found to be in the range of $\mu_c = (1000-1110)$ MeV in symmetric matter, and μ_c decreases at finite $\delta\mu$. We can compare these values with the highest baryon chemical potential realized during the BH formation, $\mu_B = 1300$ MeV. Then if the baryon chemical potential is larger than the QCD phase transition chemical potential, quark matter will be formed during the

BH formation. In order to conclude, however, it is necessary to examine with the EOS which includes both baryonic and quark degrees of freedom. The CP location is sensitive to the models and parameters. We have found that there are three types of possibilities of the transition to quark matter in the BH formation process. When the thermodynamical trajectory go below, above, or through CP in asymmetric matter, the QCD phase transition proceeds via the first order transition, the cross over transition, or the CP sweep. When CP is swept, the density fluctuation should grow, and we can expect various effects around CP such as the baryon density fluctuations, focusing of thermodynamical trajectories, disappearance of the sound mode, as discussed for the beam energy scan at RHIC [7].

It is a big challenge to construct an EOS which is applicable to the dynamical simulation of the core-collapse processes, contains both the hadronic and quark degrees freedom, and includes CP of QCD. There is an attempt to include both quark and baryon contributions based on the PQM [38]. In that work, the vacuum quark contribution is ignored and the QCD phase transition becomes the first order in the two-flavor chiral limit. It may be also necessary to consider the effects of inhomogeneous phases [39], which may emerge around the first order phase boundary.

[1] M. Asakawa and K. Yazaki, Nucl. Phys. A **504** (1989) 668.
[2] Y. Aoki, G. Endrodi, Z. Fodor, S. D. Katz and K. K. Szabo, Nature **443** (2006) 675.
[3] Z. Fodor and S. D. Katz, JHEP **0203** (2002) 014; S. Ejiri, C. R. Allton, S. J. Hands, O. Kaczmarek, F. Karsch, E. Laermann and C. Schmidt, Prog. Theor. Phys. Suppl. **153** (2004) 118; R. V. Gavai and S. Gupta, Phys. Rev. D **71** (2005) 114014; P. de Forcrand, S. Kim and O. Philipsen, PoS **LAT2007** (2007) 178; P. de Forcrand and O. Philipsen, JHEP **0811** (2008) 012.
[4] T. Z. Nakano, K. Miura and A. Ohnishi, Phys. Rev. D **83** (2011) 016014; Prog. Theor. Phys. **123** (2010) 825; K. Miura, T. Z. Nakano, A. Ohnishi and N. Kawamoto, Phys. Rev. D **80** (2009) 074034; K. Miura, T. Z. Nakano and A. Ohnishi, Prog. Theor. Phys. **122** (2009) 1045.
[5] M. A. Stephanov, PoS **LAT2006** (2006) 024.
[6] M. M. Aggarwal *et al.* [STAR Collaboration], Phys. Rev. Lett. **105** (2010) 022302.
[7] M. A. Stephanov, K. Rajagopal and E. V. Shuryak, Phys. Rev. Lett. **81** (1998) 4816; D. T. Son and M. A. Stephanov, Phys. Rev. D **70** (2004) 056001; H. Fujii, Phys. Rev. D **67** (2003) 094018; M. A. Stephanov, Phys. Rev. Lett. **102** (2009) 032301; Y. Minami and T. Kunihiro, Prog. Theor. Phys. **122** (2010) 881.
[8] M. A. Stephanov, K. Rajagopal and E. V. Shuryak, Phys. Rev. D **60** (1999) 114028.
[9] T. Hatsuda, Mod. Phys. Lett. **A2** (1987) 805.
[10] I. Sagert *et al.*, Phys. Rev. Lett. **102** (2009) 081101.
[11] H. Shen, H. Toki, K. Oyamatsu and K. Sumiyoshi, Nucl. Phys. A **637** (1998), 435; Prog. Theor. Phys. **100** (1998), 1013.
[12] A. Heger, C. L. Fryer, S. E. Woosley, N. Langer and D. H. Hartmann, Astrophys. J. **591** (2003) 288; K. Maeda and K. Nomoto, Astrophys. J. **598** (2003) 1163; K. Nomoto et al., in *Supernova 1987A: 20 Years After: Supernovae and Gamma-Ray Bursters* (2007), arXiv:0707.2187.
[13] K. Sumiyoshi, S. Yamada, H. Suzuki and S. Chiba, Phys. Rev. Lett. **97** (2006) 091101.
[14] K. Sumiyoshi, S. Yamada and H. Suzuki, Astrophys. J. **667** (2007) 382.
[15] K. Sumiyoshi, C. Ishizuka, A. Ohnishi, S. Yamada and H. Suzuki, Astrophys. J. Lett. 690 (2009) 43.
[16] C. Ishizuka, A. Ohnishi, K. Tsubakihara, K. Sumiyoshi and S. Yamada, J. Phys. G **35** (2008), 085201.
[17] J. M. Lattimer and F. D. Swesty, Nucl. Phys. A **535** (1991) 331.
[18] K. Nakazato, K. Sumiyoshi, H. Suzuki and S. Yamada, Phys. Rev. D **78** (2008) 083014 [Erratum-ibid. D **79** (2009) 069901]; Phys. Rev. D **81** (2010) 083009.
[19] Y. Nambu and G. Jona-Lasinio, Phys. Rev. **122**, 345 (1961); Y. Nambu and G. Jona-Lasinio, Phys. Rev. **124**, 246 (1961); U. Vogl and W. Weise, Prog. Part. Nucl. Phys. **27**, 195 (1991); S. P. Klevansky, Rev. Mod. Phys. **64**, 649 (1992); T. Hatsuda and T. Kunihiro, Phys. Rept. **247**, 221 (1994); M. Buballa, Phys. Rept. **407**, 205 (2005).
[20] P. N. Meisinger and M. C. Ogilvie, Phys. Lett. B **379**, 163 (1996).
[21] K. Fukushima, Phys. Lett. B **591**, 277 (2004).
[22] C. Ratti, M. A. Thaler and W. Weise, Phys. Rev. D **73**, 014019 (2006);S. Roessner, C. Ratti and W. Weise, Phys. Rev. D **75**, 034007 (2007); C. Sasaki, B. Friman and K. Redlich, Phys. Rev. D **75**, 074013 (2007).
[23] K. Kashiwa, H. Kouno, M. Matsuzaki and M. Yahiro, Phys. Lett. B **662**, 26 (2008).
[24] B. J. Schaefer, J. M. Pawlowski and J. Wambach, Phys. Rev. D **76** (2007) 074023.
[25] V. Skokov, B. Friman, E. Nakano, K. Redlich and B. J. Schaefer, Phys. Rev. D **82**, 034029 (2010)
[26] D. T. Son and M. A. Stephanov, Phys. Rev. Lett. **86** (2001) 592. J. B. Kogut and D. K. Sinclair, Phys. Rev. D **66** (2002) 034505; M. D'Elia and F. Sanfilippo, Phys. Rev. D **80** (2009) 014502; P. Cea, L. Cosmai, M. D'Elia, C. Manneschi and A. Papa, Phys. Rev. D **80** (2009) 034501; Z. Zhang and Y. X. Liu, Phys. Rev. C **75** (2007) 064910.
[27] H. Abuki, M. Ciminale, R. Gatto, N. D. Ippolito, G. Nardulli and M. Ruggieri, Phys. Rev. D **78**, 014002 (2008); H. Abuki, R. Anglani, R. Gatto, G. Nardulli and M. Ruggieri, Phys. Rev. D **78**, 034034 (2008).
[28] T. Sasaki, Y. Sakai, H. Kouno and M. Yahiro, Phys. Rev. D **82**, 116004 (2010)
[29] T. Hatsuda and T. Kunihiro, Prog. Theor. Phys. **74**, 765 (1985).
[30] M. Kitazawa, T. Koide, T. Kunihiro and Y. Nemoto, Prog. Theor. Phys. **108**, 929 (2002).
[31] Y. Sakai, K. Kashiwa, H. Kouno, M. Matsuzaki and M. Yahiro, arXiv:0902.0487 [hep-ph].
[32] D. Blaschke, J. Berdermann and R. Lastowiecki, Prog. Theor. Phys. Suppl. **186** (2010) 81.
[33] V. A. Dexheimer and S. Schramm, Nucl. Phys. Proc. Suppl. **199** (2010) 319.
[34] P. Demorest, T. Pennucci, S. Ransom, M. Roberts and J. Hessels, Nature **467** (2010) 1081.
[35] A. Ohnishi, D. Jido, T. Sekihara and K. Tsubakihara, Phys. Rev. C **80** (2009) 038202.
[36] K. Sumiyoshi, S. Yamada, H. Suzuki, H. Shen, S. Chiba and H. Toki, Astrophys. J. **629** (2005) 922.
[37] J. A. Pons, S. Reddy, M. Prakash, J. M. Lattimer and J. A. Miralles, Astrophys. J. **513** (1999) 780; J. A. Pons, J. A. Miralles, M. Prakash and J. M. Lattimer, Astrophys. J. **553** (2001) 382.
[38] J. Steinheimer, V. Dexheimer, H. Petersen *et al.*, Phys. Rev. C **81** (2010), 044913; J. Steinheimer, S. Schramm, H. Stocker, J. Phys. G **38** (2011), 035001.
[39] E. Nakano and T. Tatsumi, Phys. Rev. D **71** (2005) 114006; D. Nickel, Phys. Rev. D **80** (2009) 074025; T. Kojo, Y. Hidaka, L. McLerran and R. D. Pisarski, Nucl. Phys. A **843** (2010) 37.